國立臺灣大學電機資訊學院生醫電子與資訊學研究所
碩士論文

Graduate Institute of Biomedical Electronics and Bioinformatics

College of Electrical Engineering and Computer Science

National Taiwan University

Master Thesis

高品質同時量測人腦血液動力信號與電生理信號方法

A method of concurrent high quality measurement of hemodynamic and electrophysiological signals of the human brain

黃書璵

Shu-Yu Huang

指導教授：鍾孝文博士，林發暄 博士

Advisor: Hsiao-Wen Chung, Ph.D., Fa-Hsuan Lin, Ph.D.

中華民國 107 年 12 月

Dec, 2018

Acknowledgement

中文摘要

　　腦電圖以及功能性核磁共振影像都是非侵入式神經顯影方式，它們分別提供了毫秒等級的時間解析度的神經反應以及毫米等級的空間解析度。在測量兩者資料時，可以是分開量測或同時量測。在實驗需要特別排除因記憶或學習效應造成的影響時，同時量測腦電圖和功能性磁振影像可以排除因兩次量測間差異造成的偏差。可是在同時收錄腦電圖及功能性磁振影像時腦電圖會受到在高磁場下的心搏產生的心搏假影及梯度線圈開關產生的梯度假影劇烈影響。因梯度假影的大小百倍於神經反應，並且梯度假影對受試者移動敏感，在經過信號處理減除梯度假影後，其殘值仍會影響腦電圖的品質。為降低梯度假影影響，我們提出將快速的 simultaneous multi-slice inverse imaging(SMS-InI)序列和腦電圖間歇掃描。可預期在沒有掃描的區間(每 2 秒鐘內的 1.9 秒)可以提升腦電圖的品質，同時 SMS-InI 也維持與傳統 Echo Planar Image(EPI)同等級的靈敏度及空間解析度。經由時頻分析我們知道使用傳統 EPI 序列造成的梯度假影會在固定頻率有最大的影響，所以我們激發 15 赫茲穩態視覺相關電位以比較間歇同時量測 SMS-InI 的腦電圖與同時量測傳統 EPI 的腦電圖及的品質。我們使用 SMS-InI 及腦電圖的間歇掃描量測到可以與在磁振造影室外量測的腦電圖相比的 15 赫茲穩態視覺相關電位以及可以與 EPI 相提並論的血動力反應圖。此種間歇式掃描腦電圖及 SMS-InI 可適用於對腦電圖品質較有要求的實驗，例如讓功能性磁振影像使用發作間期癲癇樣放電(inter-ictal discharges, IID)時間點定位癲癇病患在大腦中激發放電的位置。

關鍵字：同時量測、腦電圖、功能性磁振造影、快速造影、間歇

Abstract
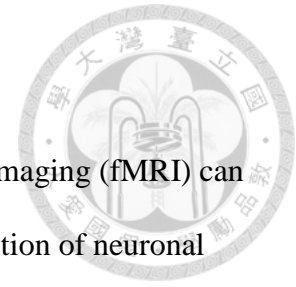
Electroencephalography (EEG) and functional magnetic resonance imaging (fMRI) can be combined to provide millisecond resolution and millimeter resolution of neuronal and hemodynamic activity. EEG and fMRI can be recorded concurrently or separately for data integration. In experiments considering memory or learning effects, concurrent EEG-fMRI is preferable to avoid bias due to separate measurements. In concurrent EEG-MRI recording, EEG is heavily distorted by pulse artifacts, which are caused by heartbeats in a strong magnetic field, and gradient artifacts, which are caused by repetitive gradient coil switching during MRI acquisition. Because GA is hundreds times larger than typical evoked neuronal responses and GA is very sensitive to movements, the residue of GA after GA suppression can significantly degrade EEG quality.

We propose to interleave simultaneous multi-slice inverse imaging (SMS-InI) concurrently with EEG. In this way, EEG recorded with gradient-artifact-free intervals (1.9 s in every 2-s) is expected to have high quality, while SMS-InI provides comparable sensitivity and spatiotemporal resolution like EPI. We used SMS-InI-EEG to measure 15-Hz steady-state visual evoked potentials comparable with EEG recorded outside MRI and the hemodynamic responses comparable with EPI.The interleaved SMS-InI-EEG can be applied to measurements sensitive to EEG quality, such as localizing irritative zones of inter-ictal discharges (IID) in epilepsy patients using fMRI based on IID timing.

Key words: concurrent, EEG, fMRI, SMS-InI, interleaved

Outline

List of Figures

List of Tables

Chapter 1. Introduction

Electroencephalography (EEG[1-3]) and functional magnetic resonance imaging (fMRI [2, 4, 5]) can non-invasively provide millisecond resolution and millimeter resolution of neuronal and hemodynamic activity, respectively [5-7]. However, EEG and MRI have their specific challenges. The spatial resolution of the neuronal activity estimated using EEG is uncertain and coarse (in the range of 6 and 10 mm [8]). Estimated EEG sources are only relatively accurate at cortical surface [1-3]. On the other hand, the hemodynamic responses recorded by fMRI is temporally slow: the time from the onset of an activation to the peak timing is about a few seconds. It takes about 20 s to 30 s to return to the baseline [9, 10]. Functional MRI does not detect the neuronal activities directly but the accompanied hemodynamic responses [5, 10]. To estimate both the temporal and the spatial distribution of neuronal events, EEG and fMRI can be combined. There are three ways of integrating EEG and fMRI: (i) Estimate the onset and duration of neuronal events by EEG, then fMRI data use this timing information to estimate the areas of brain activities related to these events [11-13]. (ii) Estimate the areas of the hemodynamic activities by fMRI, then mathematically constrain the neuronal source estimated by EEG within these areas [14-16]. (iii) Estimate the interaction relationship between neuronal response and hemodynamic response from the collection of EEG and fMRI data [17-19].

Though EEG data can be integrated with fMRI data in many ways, their data can be acquired separately or concurrently. Concurrent EEG and fMRI is preferable when learni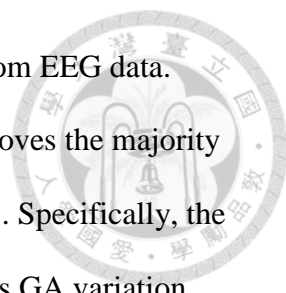ng and memory effect lead to crucial biases in the experiment[13, 20]. Specifically, repeated stimulation leads to memory and learning effects, so the brain activities and behaviors can be different between separate EEG and fMRI experiments

[13, 20-22]. Though preferable in some cases, concurrent EEG-MRI needs MRI compatible EEG devices. For example, the electrodes of EEG must be nonmagnetic in order to minimize projectile hazards. Metallic EEG electrodes also cause concerns in local heating, MRI signal loss, and image distortion [13]. These challenges can be mitigated by avoiding using dry EEG electrodes and avoiding close loops between electrodes and wiring [13, 23].

In addition to concerns described above, EEG measured concurrently with MRI is heavily distorted [6, 7, 13, 24, 25]. Two most serious EEG artifacts are gradient artifact (GA [7, 25, 26]) and pulse artifact (PA [6, 7, 24]). GAs are the electric motive force (EMF) on the EEG electrodes induced by the repetitive gradient switching of scanning [13]. PAs are the EMF on the EEG electrodes induced by (i) the vibration caused by heart beats under high-field in MRI, or (ii) the local field change caused by cerebral blood flow [13]. During echo-planar imaging (EPI [4, 27]) in a 3T MRI, the GA can be as strong as 3 millivolts [13], and the PA is about 200 microvolts [6, 7, 24]. In contrast, spontaneous brain waves, such as 8~12Hz alpha rhythm, are only in the rage between 50 and 100 microvolts [28]. Visual evoked potentials are in the rage between 4 and 10 microvolts [29-33]. GA and PA are far larger than spontaneous and evoked brain activities. GA and PA need to be removed in order to isolate the neuronal responses [7, 26].

Signal processing methods have been proposed for the GA and PA removal. Band filtering methods were used to decrease the signals in the frequency bands related to GA and PA ([26, 34]: GA , [35]: PA), but the neuronal signals overlapping the frequency of GA (5~2500Hz [24]) or PA(<20Hz [24]) may also be removed [36]. GA and PA can be removed by identifying their distinctive patterns. The most common method for GA removal is averaging EEG segments during successive MRI repetitions

8

and to generate a GA template. Then we subtract the GA template from EEG data. Though this average artifact subtraction (AAS, [25, 36]) method removes the majority of GA, it cannot deal with EEG with variation of GA effectively [37]. Specifically, the subject movement cause GA variation during the MRI scan [37]. This GA variation results in GA residuals in EEG after AAS. Consequently, the EEG is still deteriorated. PA can be removed by methods similar to AAS [24, 36]. Considering variable PA across cardiac periods, a PA template can be derived from a few major components of Principle Component Analysis of EEG synchronized to cardiac peaks [36].

Note that the PA removal is typically after the GA removal, because of their difference in amplitudes. Thus, the GA residuals can be remained after PA removal [36]. To account for this challenge, interleaved EEG-MRI has been proposed [7, 13, 35, 38-40]. Interleaved EEG-MRI attempts to collect EEG during intervals without MRI gradient coil switching in order to minimize GA [7, 13, 35, 38-40]. The GA and their residuals occur at harmonics of the slice selection frequency (10~20 Hz) convolved with harmonics of the volume repetition frequency (1/TR; 0.2~2Hz) [41, 42]. These frequencies can overlap with the frequency bands of neuronal activity (0.4~50Hz) [5-7]. Interleaved EEG-MRI can reduce the deterioration of EEG quality due to MRI at these frequencies. Interleaved EEG-MRI cannot prevent PA. Implementing interleaved fMRI-EEG with EPI needs to trade-off between the MRI spatiotemporal resolution and field of view (FOV). Using EPI, a typical repetition time (TR; about 2 seconds) is crowded with MRI gradient coil switching due to the required FOV and spatial resolution (~ 3 mm). Thus, the proportion of time in each TR without gradient coil switching is very small. This difficulty may be addressed by reducing the number of slices [13, 39]. Yet the compromised FOV may not be acceptable in experiments requiring whole-brain coverage. While it is possible to use much longer TR to allow for longer MRI gradient

9

coil silent intervals without compromising the FOV and resolution, it may not capture

the hemodynamics effectively due to failing the Nyquist sampling requirement [13, 35,

38]. Taken together, interleaved EEG-MRI using EPI needs to trade-off between fMRI

spatiotemporal resolution, FOV, and EEG quality.

To address this challenge, we propose to interleave simultaneous multi-slice

(SMS [43]) inverse imaging (InI [44]) and EEG. InI reconstruct the information in the

direction of slice selection by weighting the image of multiple head coils by spatial

sensitivity (**Figure 1**) [44]. Only one excitation is needed for a whole brain InI, but the

lack of slice selection gradient encoding makes InI blurred in the direction of slice
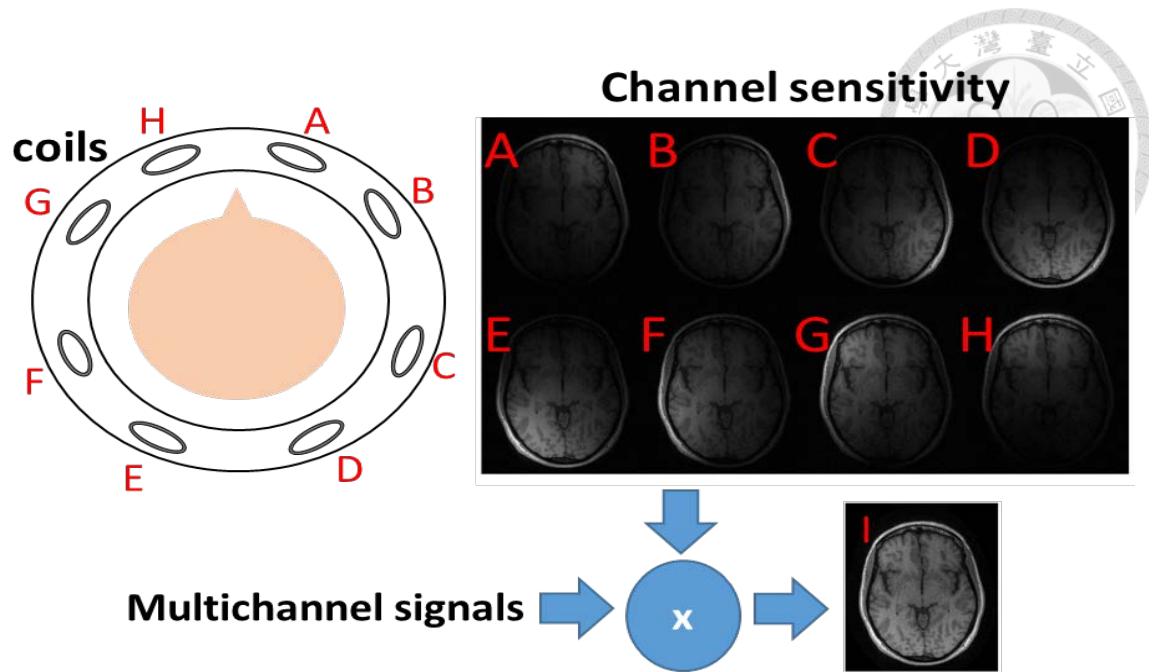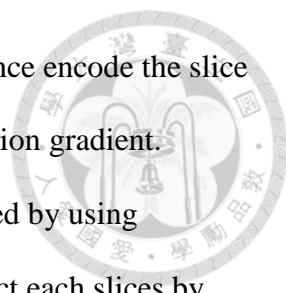
selection [44].

10

Figure 1 Illustration of InI reconstruction. A,B,C,D,E,F,G,H marks spatially distributed coils and their sensitivity map, and each coil is less sensitive to distant areas. Multichannel signal was weighted by individual sensitivity and summed to form the complete image (I).

SMS was combined to ameliorate this drawback. SMS sequence encode the slice direction information by exciting multiple slices with one slice selection gradient. Though the images of each slices were overlaid, they can be untangled by using blipped-CAIPI EPI [45] trajectory to shift each slices, then reconstruct each slices by sensitivity encoding (SENSE[46]) using sensitivity map of multiple head coils. Two different slice sets were separated by simultaneous echo refocusing (SER) in this work for better spatial resolution(**Figure 2**[44])[47]. Combining InI with SMS, SMS-InI can achieve 5 mm isotropic resolution in 0.1 s with whole-brain coverage at 3T using a 64-channel head coil array [44]. Integrating SMS-InI with TR = 2 s, we have 1.9 s (95% of duty cycle) without MRI gradient switching and EEG without GA. To test this approach, we study the 15-Hz steady state visual evoked potential (SSVEP [48-50]) elicited by visual stimuli flashing at 7.5 Hz measured concurrently with EPI and SMS-InI. SSVEP has oscillatory responses at harmonics of the stimulation frequency at the visual cortex [48-50].

Because the SSVEP at 15 Hz overlaps with GA in our EPI-EEG protocol, we can empirically assess how interleaved SMS-InI-EEG affects the quality of SSVEP. We hypothesize that the SSVEP at 15 Hz can be better identified from interleaved SMS-InI-EEG measurements than from EPI-EEG measurements, because the GA is not overlapping with the evoked oscillatory neuronal responses.

12
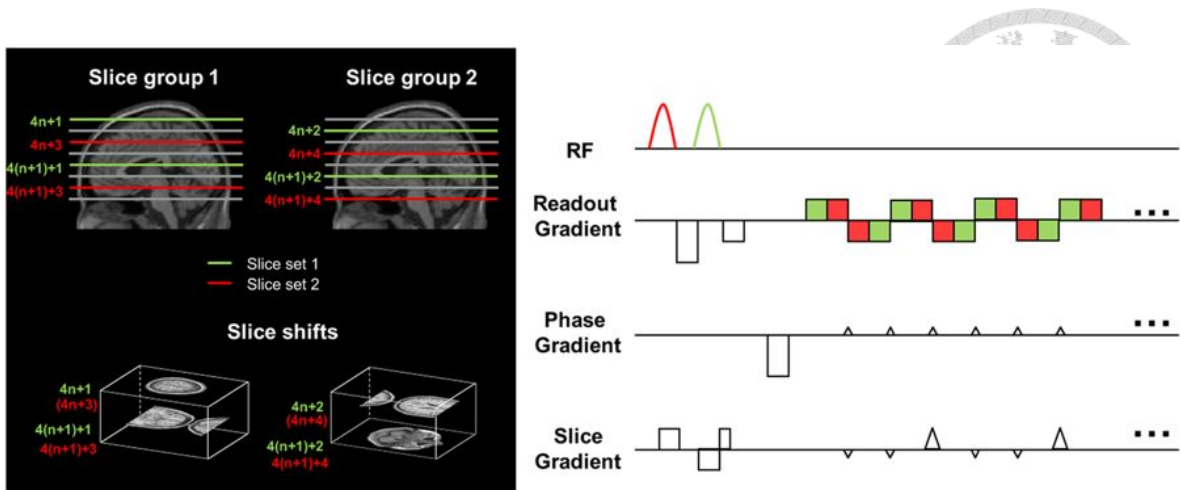
Figure 2 Slice prescription (left) and pulse sequence diagram (right) of SMS-InI [44]..

The acquisition used two slice groups, each of which had two slice sets. Two different

slice sets were separated by simultaneous echo refocusing (SER). Adjacent slices within

the same slice set were shifted by blipped-CAIPI EPI with 1/3 FOV shift. These shifted

slices were then separated by coil sensitivity information. The acquisition time for each

slice group was 50 ms.

Chapter 2. Methods

2-1. MRI acquisition

All MRI data was measured on a 3T system (Skyra, Siemens, Munich, Germany) with a 64-channel head coil array. Structural images were acquired with the MPRAGE pulse sequence (TR/TE=2530/3.03 ms, resolution= 1x1x1 mm^3, FOV = 256 mm, flip angle = 7°, matrix size = 224×256, GRAPPA acceleration = 2). Functional images were acquired with a SMS-InI sequence (TR/TE = 50/30 ms, FOV=210 mm, flip angle = 30°, resolution = 5x5x5 mm^3, slice numbers = 24). It took two excitations for SMS-InI to cover the whole brain, and the acquisition time per brain volume was 100 ms. Between two consecutive SMS-InI scans, there was an interval of 1.9 s (95% of duty cycle) without any MRI acquisitions. There was no GA on EEG in this interval. In comparison, we also acquired T_2^*-weighted EPI (TR/TE = 2000/36 ms, FOV = 224 x 224 x 123 mm, flip angle = 90°, slice numbers = 30, image matrix size = 64 x 64 x 32, GRAPPA acceleration = 2). The induced gradient artifact of each acquisitions protocols were illustrated in **Figure 1**.

14

Figure 3 The GA elicited by EPI and SMS-InI. The black dash lines indicate the

beginning of each SMS-InI scan. The green line indicates the EEG from EPI-EEG. The

blue line indicates the EEG from SMSInI-EEG.
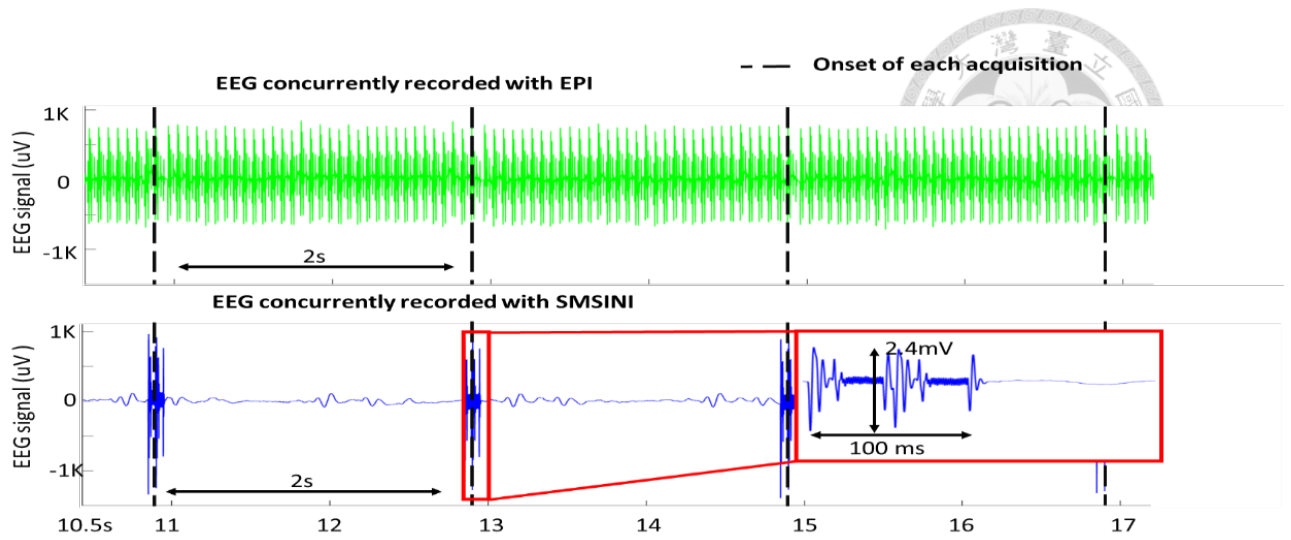
15

2-2. EEG acquisition

EEG was measured by an MR-compatible system (BrainAmp MR Plus, Brain Products, Gilching, Germany) with a 32-channel EEG cap (BrainCap MR, Brain Products, Gilching, Germany). Locations of electrodes followed the 10-20 standard (Fp1, Fp2, F3, F4, C3, C4, P3, P4, O1, O2, F7, F8, T7, T8, P7, P8, Fz, Cz, Pz, Oz, FC1, FC2, CP1, CP2, FC5, FC6, CP5, CP6, TP9, TP10, POz). EEG data were referenced with respect to FCz. The ground reference was at the AFz electrode. The electrocardiogram (ECG) was also measured by placing an electrode at the back of the participant. The EEG data were sampled at 5 kHz without online filtering and was synchronized to the MR scanner at the beginning of each RF excitation via a TTL trigger signal [36, 51]. The impedance of each electrode was controlled to be lower than 4 kΩ after applying conductive paste. The cap wire was straightened and fixed along the main magnetic field for 50 cm and connected to an EEG amplifier in the MRI bore. This setup was meant to reduce the GA induced by the wire [51]. Electrode positions were measured by a digitizer (Fastrak, Polhemus, Vermont, Canada) to register EEG electrodes with the head model derived from structural MRI.

2-3. Participant and Instructions

Nine healthy participants with written inform consents approved by the Institute Reviewing Board from National Taiwan University Hospital were recruited to this study (5 males, all right-handed, corrected to normal vision with contact lenses). The participant was instructed to keep visual fixation at a cross hair at the center of the screen, and press a button with their right index finger when the crosshair changed its color from black to red. This task was meant to ensure participants' eyes fixating at the center of the screen. Red crosshair appeared for 1 s randomly and independently from

the onsets of checkerboard flashing. During the experiment, checker board patterns

flashing at 7.5 Hz were shown to participants randomly with a minimal inter-stimulus

interval of 2 s. Stimulus duration was 1 s. The stimuli subtended 4.3° of visual angle

and contained 24 evenly distributed radial wedges and eight concentric rings of equal

width. Such visual stimuli were used to generated SSVEP peaked at 15 Hz. To avoid

GA on SSVEP in SMS-InI-EEG, onsets of checkboard flashing were temporally jittered

between 0.2 s and 0.9 s after the beginning of each SMS-InI scan (Figure 1).

We had three EEG-fMRI protocols: EPI-EEG, SMS-InI -EEG, and EEG

recorded in the MR scanner without any MRI scan (EEG-only). Three runs of data were

collected for each protocol. Each run lasted for 8 minutes. Totally 50 trials of

checkerboard flashing were presented to the participants in each run for each protocol.

The stimuli were presented using E-Prime 2.0 (E-Prime 2.0.10.242 Professional,

Psychology Software Tools, Sharpsburg, USA).

2-4. EEG preprocessing

The EEG processing started from artifacts suppression using the published procedure [24]

implemented in MATLAB (MATLAB 2015a, Mathworks®, Natick, Massachusetts,

U.S.A) with the help of fMRIb toolbox (fMRIb v2.00, Oxford Center for Functional MRI

of the Brain, Oxford, U.K. [24]). For EPI-EEG and SMS-InI-EEG, these procedures

included: GA suppression by averaging artifact subtraction (AAS [25], **Appendices** A),

1~50-Hz zero-phase band-pass filtering, down-sampling to 500 Hz, heart beat detection

(**Appendices** B), PA suppression by the optimal basic set method (OBS[36], **Appendices**

C), removal of the global mean from the time series of individual electrodes, and re-

referencing of EEG data by subtracting the electrodes-averaged EEG time series from the

EEG time series at each electrode. Note that the GA waveform was separately modeled

17

by averaging EEGs recorded during SMS-InI and EPI scans. For EEG-only scan, we followed the same data processing except that AAS was skipped.

SSVEP was separately calculated for the three protocols by taking the average waveform between 200 ms before and 1200 ms after the onset of visual checkboard flashing. Before estimating the SSVEP, the constant and the linear drift in each epoch was removed by linear regression. Epochs with the maximal EEG over 700 uV were excluded.

2-5. EEG source estimation

The sources of SSVEPs were estimated for assessing the in-band SNR in the interested V1 and V2 area. T_1-contrast brain MRI was used to separate the brain into the white matter and gray matter (FreeSurfer, Oxford Center for Functional MRI of the Brain, Oxford, U.K [52]). Then, we used MNE toolbox [53]to build 3D brain models, including the scalp, skull, and brain compartments with boundary element method [54]. The locations of EEG electrode were registered to the 3D scalp model. In order to solve the EEG forward problem, the source space was constructed on the cortical surface at 9,753 locations to model 29,259 equivalent current dipoles (ECDs; 3 orthogonal ECDs at each location) with 4 mm spatial resolution. The gain from each of three orthogonal ECDs at each source location to each EEG electrode was then calculated by Helsinki BEM Framework LCISA solver for MEG/EEG (LCISA v160405, Department of Neuroscience and Biomedical Engineering of Aalto University, Aalto, Finland [54, 55]). We estimated the EEG current source with the minimum-norm estimate method[44] without constraining the current dipole orientation. Finally, the estimated current density distribution was projected to the MNI coordinate system with MNE toolbox [53] for group analysis.

18

2-6. Functional MRI preprocessing

The SMS-InI data was first reconstructed to create brain volumes once every 0.1 s. We excluded the first 3 measurements of each runs of SMS-InI or EPI to ensure that the magnetization reached a steady state. Then the SMS-InI data were motion corrected, co-registered to individual high-resolution brain anatomy, and spatially projected to the MNI coordinate system. EPI data were preprocessed by slice-timing correction, intra-session 3D motion correction, co-registration between fMRI and MPRAGE data, converting to cortical surface space, and spatially projected to the MNI coordinate system. EPI and SMI-InI were both spatial smoothed using an isotropic Gaussian kernel of 5-mm full-width-half-maximum. The constant and linear drift of each image vertex's the time series was removed by regression. These pre-processing steps were done by Statistical Parametric Mapping (SPM12, Welcome Department, University College London, UK[56]) implemented in Matlab (version R2015a, MathWorks, Sherborn, MA, USA). MPRAGE MRI was used to generate the cortical surface space by FreeSurfer toolbox(freesurfer-Linux-centos4_x86_64-stable-v5.1.0-20110514, Oxford Center for Functional MRI of the Brain, Oxford, U.K[52]).

2-7. EEG evaluation

Spectral analysis was done to demonstrate the trait of GAs in SMS-InI-EEG and EPI-EEG. The spectrograms were then calculated at each brain location using Discrete Gabor Transform (DGT [57]) using a 2-s sliding window with a 40-ms time grid and 1 Hz frequency grid, we evaluate the power of our result in the range of 15 Hz. To assess the quality of EEG acquired in different protocols, we measured the SNR at the visual

19

cortex. This assessment was done separately for EEG sources collected by SMS-InI-EEG, EPI-EEG and EEG-only protocols. Specifically, we used the EEG source ($x(n)$, where n denotes the time points) between 250 ms to 1200 ms as the signal part ($n \in N_s$, with N_s time points) and EEG source 200 ms to 0 ms before stimuli as the noise part ($n \in N_n$, with N_n time points) to compare the performance between the SMS-InI-EEG, the EPI-EEG, and the EEG-only case. The low frequency pink noise ($1/f^\alpha$ spectrum[57]) in SSVEP was removed by first-order backward differencing [58] before time-frequency analysis. The spectral power were calculated at V1 and V2 with wavelet transform (WT) using a 5-units width Morlet wavelet [59]. We calculated the averaged normalized spectral power at 15Hz. SNR was calculated as the average of power of EEG source $P(m, n) = |WT(x(n))|^2$ in the signal part, where m indicated the different frequencies, divided by the average of power of EEG source in the noise part.

$$\text{SNR} = 20 \log\left(\left(\sum_{n \in N_s} \frac{P(M,n)}{N_s}\right) / \left(\sum_{n \in N_n} \frac{P(M,n)}{N_n}\right)\right) \qquad \text{Eq. 1}$$

With M=15Hz. To assess how the residue of GA distributed in the cortex, we also calculated the power of noise in the 15Hz.

$$\text{Noise} = 20 \log\left(\sum_{n \in N_n} \frac{P(M,n)}{N_n}\right) \qquad \text{Eq. 2}$$

2-8. Data analysis of EPI and SMS-InI

Functional MRI measured by SMS-InI or EPI were analyzed by General Linear Model (GLM[60]). The hemodynamic response model was built by convolving a two gamma hemodynamic response function [5, 10] with the paradigm of stimulus onsets. Confounds of linear drift, run-specific constant shift, head motion, and the global mean of each instantaneous measurements across the whole head were included in the GLM to model nuisance disturbances. The significance of the size of the hemodynamic responses was estimated with one-sample t-test for each brain location separately. The

20

p-values were corrected for multiple comparison by controlling the false discovery rate (FDR[61]).

21

Chapter 3. Results

3-1. EEG results

While GA deteriorated the 15 Hz frequency band in EPI-EEG, the SMS-InI-EEG was expected to be much less affected by GA between 200 ms and 1900 ms after the onset of each SMS-InI scan (**Figure 4. B**).

The spectrogram of the SSVEP at the visual cortex was found similar between SMS-InI-EEG and EEG-only protocols (**Figure 5**), especially in the frequency band of the expected neuronal events (15Hz). EEG from SMS-InI-EEG and EEG-only showed clear oscillatory features of SSVEP at 15 Hz between 250 ms and 1200 ms. On the contrary, EEG from the EPI-EEG showed no obvious 15 Hz oscillation.

The average SNR of SMSInI-EEG was 15.04 dBs which was 5.48 times higher than the SNR of EPI-EEG in the visual cortex (7.66 dB; $p < 0.00001$), and not so different from the SNR of EEG-only case (15.17 dB; p>0.05). The SSVEP from SMS-InI-EEG showed more regions with SNR higher than 11 dB in the visual cortex than from EPI-EEG (**Figure 6**, **Table 1**). The EPI-EEG had 15 Hz noise higher than 90% of the areas in the lateral cerebral fissure, uncus, hippocampal gyrus, and intraparietal sulcus (**Figure 7**). The areas with higher SNR beyond visual cortices in EPI-EEG were not overlapped with the areas with higher 15Hz noise.

22
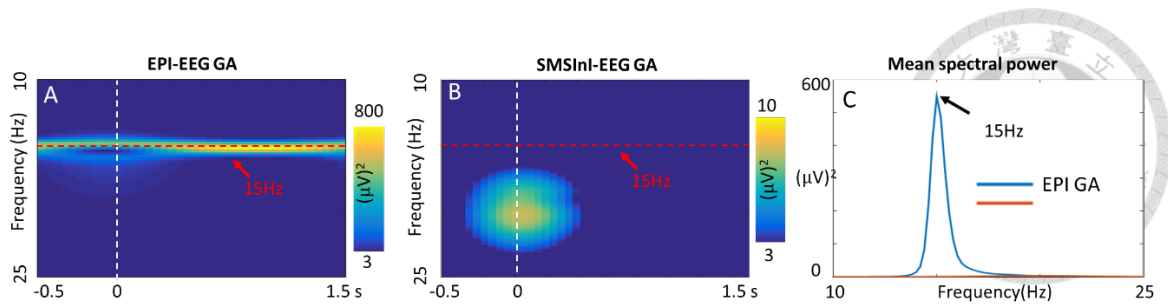
Figure 4 GA spectrogram of EPI-EEG (A) and SMS-InI-EEG (B) at electrode Oz. The spectrogram was calculated between -500 ms and +1500 ms with respect to the onset of each MRI volume scan (white dashed line). The 15Hz frequency of EPI slice selection was marked as red dashed line.(C) The average spectral power of EPI-EEG and SMSInI-EEG at electrode Oz between +200 and +1900 ms after the onset of each MRI volume scan.

23
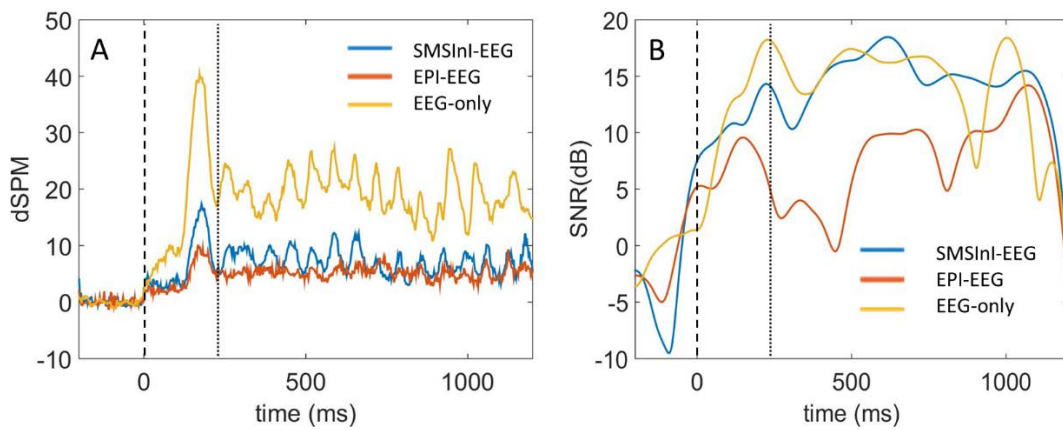
Figure 5 SSVEP (left) and its spectrogram (right). SNR was defined as the ratio of the average spectral power in the interval after (between +250 ms and +1200 ms) and before (between -200 ms and 0 ms) visual stimulus onset. The 15-Hz oscillation was observed between +250 ms and +1200 ms in EEG-only (yellow trace). This oscillation was also clearly observed in SMS-InI-EEG (blue trace) but less visible in EPI-EEG (red trace).

24
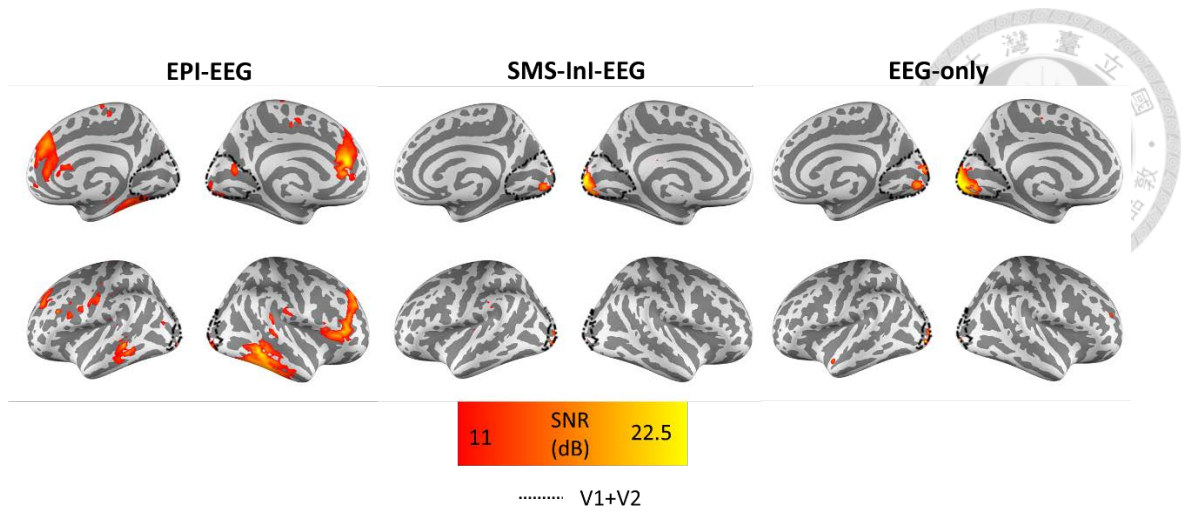
Figure 6 SNR maps of SSVEP from EPI-EEG (left), SMS-InI-EEG (middle), and EEG-only (right). Only SNR higher than 11 dB was color- coded and displayed. High 15-Hz SNR was localized near the calcarine sulcus in the primary visual cortex (V1) in both SMS-InI-EEG and EEG-only protocols. EPI-EEG had much smaller 15-Hz SNR region in the visual cortex and had a high 15-Hz SNR in the frontal lobe.

SMS-InI-EEG

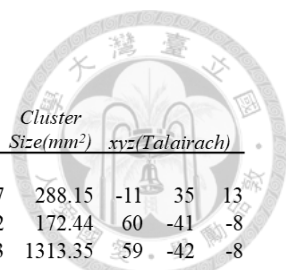|	Brain region	Max SNR(dB)	Cluster Size(mm²)	xyz(Talairach)		
L	Lateral occipital	21.017	1610.89	-14	-99	2
L	Middle temporal	20.737	29.48	-62	-17	-15
R	Pericalcarine	19.355	10.98	18	-92	2
R	Lingual	19.196	301.8	7	-90	-3
L	Lingual	19.107	11.63	-9	-73	0
L	Lateraloccipital	17.516	37.28	-19	-92	-5
L	Pericalcarine	17.062	60.95	-13	-88	9
L	Lingual	16.889	39.28	-15	-85	-5
R	Lingual	16.3	40.44	7	-84	-3
R	Cuneus	15.264	12.48	6	-90	14
R	Cuneus	15.172	14.22	8	-91	14
L	Supramarginal	14.707	10.59	-57	-32	28

EEG-only

	Brain region	Max SNR(dB)	Cluster Size(mm²)	xyz(Talairach)		
L	Lingual	22	2771	-8	-92	-2.9
L	Lingual	22	9.55	-15	-68	0.3
L	Middle temporal	21	30.11	-62	-18	-13
R	Lingual	19	281.8	5.2	-86	0
L	Middle temporal	19	7.35	-53	-21	-21
R	Pericalcarine	19	11.85	17.9	-92	3.1
R	Cuneus	18	360.4	5.3	-88	15.5
R	Lingual	18	80.92	5.2	-82	-1.3
L	Pericalcarine	18	6.87	-17	-76	10.5
R	Lateral occipital	17	17.62	29.4	-90	3.7
L	Superior temporal	17	60.46	-51	7.6	-16
L	Superior temporal	17	7.57	-51	5.5	-12
R	Cuneus	17	20.53	6.8	-89	17.5
R	Rostral middle frontal	16	26.22	25.2	40.5	16.5
R	Rostral middle frontal	15	7.63	29.7	41.2	15.3
R	Pericalcarine	15	12.57	13	-87	4.3
R	Lingual	15	5.82	13	-82	-7.2

EPI-EEG

	Brain region	Max SNR(dB)	Cluster Size(mm²)	xyz(Talairach)		
L	Rostral anterior cingulate	20.447	288.15	-11	35	13
R	Middle temporal	19.252	172.44	60	-41	-8
R	Middle temporal	19.173	1313.35	59	-42	-8
R	Parstriangularis	18.748	472.72	51	30	3
L	Rostral anterior cingulate	18.078	20.63	-6	37	11
L	Middle temporal	17.86	24.08	-53	-40	-3
R	Rostral middle frontal	17.688	441.93	25	43	27
R	Superior frontal	17.604	245.8	9	38	30
R	Superior frontal	17.578	114.53	9	38	28
L	Middle temporal	17.473	35.53	-51	-40	-3
L	Middle temporal	17.389	47.09	-58	-38	-10
R	Fusiform	17.109	267.55	41	-50	-14
R	Fusiform	16.983	51.03	30	-61	-5
R	Rostral middle frontal	16.822	71.38	41	39	20
L	Rostral middle frontal	16.792	11.94	-39	27	22
R	Inferior temporal	16.431	179.38	54	-31	-18
L	Rostral middle frontal	16.424	35.79	-25	36	27
R	Middle temporal	16.401	78.61	61	-32	-11
L	Rostral middle frontal	16.387	30.37	-25	37	28
R	Middle temporal	16.378	69.84	61	-36	-4
R	Fusiform	15.883	37.47	36	-43	-7
R	Bank ssts	15.281	18.85	62	-42	-1
L	Lateral occipital	15.203	20.15	-16	-94	-7
L	Lateral occipital	15.154	17.28	-19	-94	-8
R	Rostral anterior cingulate	15.149	14.24	7	39	5
R	Rostral anterior cingulate	15.002	11.4	9	40	4
R	Parsopercularis	14.695	16.45	48	15	8
L	Pericalcarine	14.218	14.03	-18	-67	11

Table 1 Vertex SNR peaks of SSVEP from EPI-EEG and SMS-InI-EEG. All clusters listed was larger than 10 mm² and with minimal SNR > 14 decibels.

26
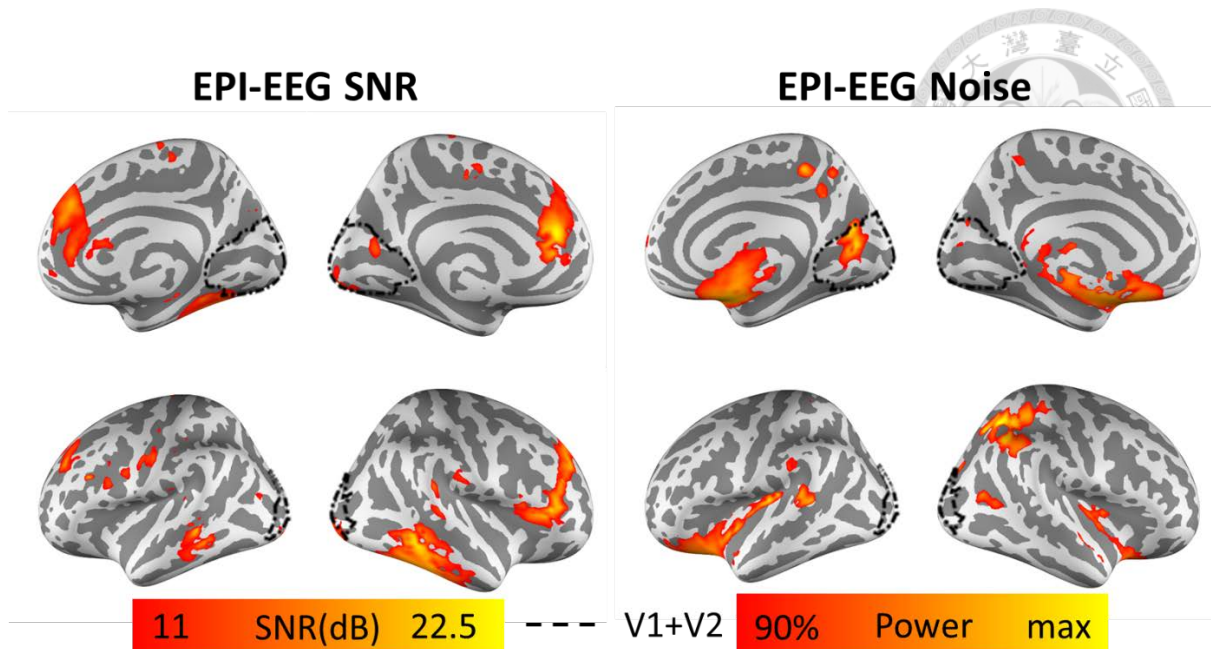
Figure 7 Comparing the SNR map (left) and noise map (right) of EPI-EEG source in 15Hz band. Only SNR higher than 11 dB and spectral power higher than 90% of the vertices was color- coded and displayed. Beyond the visual cortex, high 15-Hz SNR were localized near the frontal and temporal cortex. Beyond the visual cortex, high 15-Hz noise were localized near the lateral cerebral fissure, uncus, hippocampal gyrus, and intraparietal sulcus.

3-2. Functional MRI results

Both EPI and SMS-InI detected significant hemodynamic response in the occipital lobe (**Figure 5**). Active brain areas detected by EPI or SMS-InI were similar, including the primary and secondary visual cortex.

SMS-InI detected broader significant hemodynamic responses beyond the boarder of V1 and V2. The largest cluster of SMS-InI estimates lies in the right hemisphere and peaked in pericalcarin cortex. The largest cluster of EPI estimates lies in the left hemisphere but also peaked in pericalcarin cortex. There are some other clusters of brain areas commonly activated in SMS-InI and EPI, which included the left lingual cortex and the right lateraloccipital cortex (**Table 2**).
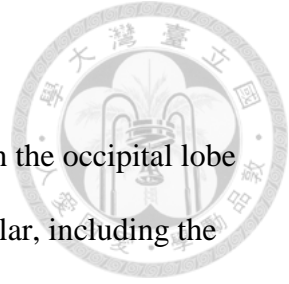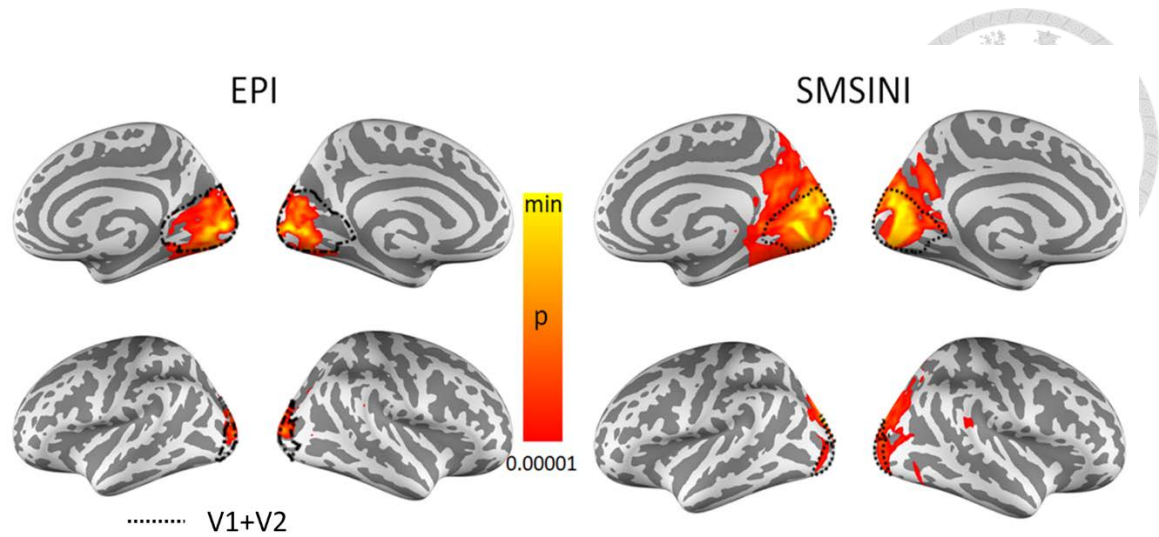
Figure 8 Significant hemodynamic responses detected by EPI and SMS-InI. All MRI data were measured on a 3T system (Skyra, Siemens) with a 64-channel head coil array. Similar BOLD signal localized at the calcarine sulcus, lingual gyrus, cuneus, and lateral occipital sulcus was observed in EPI and SMS-InI.

SMS-InI

Brain region	#voxels	Cluster Size(mm^2)	Max T value		xyz(MNI)	
R pericalcarine	9017	6452	29.9	8	-74	6
L superiorparietal	8332	5204	28.4	-19	-87	22
R precuneus	1277	635	16.8	5	-63	29
L lingual	839	819	23.5	-7	-91	-2
L precuneus	661	264	16.1	-26	-58	5
L lateraloccipital	567	389	12.1	-39	-87	-10
R precuneus	376	193	15.3	12	-63	34
R lateraloccipital	287	196	12.3	26	-89	9
R inferiorparietal	138	84	13.1	33	-82	16

EPI
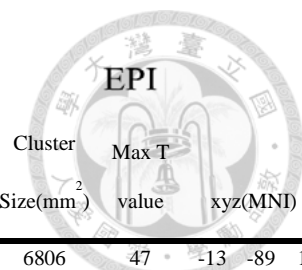
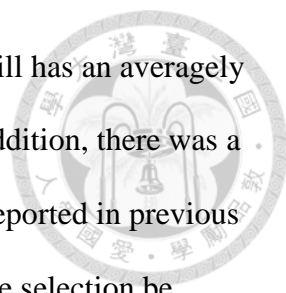| Brain region	#voxels	Cluster Size(mm^2)	Max T value		xyz(MNI)	
L pericalcarine	9477	6806	47	-13	-89	1
R pericalcarine	8282	5968	51	14	-88	5
R lateraloccipital	766	520	31	255	-88	9
L lingual	638	250	18	-24	-55	-1
L inferiorparietal	291	193	24	-31	-85	14
R cuneus	113	89.8	26	7	-74	24
R lingual	109	39	16	22	-45	-7

Table 2 Statistics of vertex T value peaks of SSVEP from EPI and SMS-InI. All clusters listed was larger than 100 voxels and with maximal corresponding p-value < 0.00001.

Chapter 4. Discussions and Conclusions

We introduced the Interleaved SMS-InI-EEG instead of EPI-EEG for compressing fMRI acquisition time while maintaining FOV and time resolution of MRI. The compression of acquisition time reduce the impact of GA on EEG, and improve SNR. We used SSVEP to verify this improvement of SNR at the frequency of reciprocal of slice selection time (15Hz). The 7.5Hz flashing checker board stimuli was used to induce the 15Hz SSVEP. The 15Hz in-band SNR of this SSVEP in the occipital is larger when using interleaved SMS-InI than using EPI-EEG. The in-band SNR was locally peaked near the calcarine sulcus in V1, and lingual gyrus, cuneus, and lateral occipital sulcus in V2 in both SMS-InI-EEG and EEG-only case. This results were accordance with the fMRI results. The resulted activated areas are the first stop of the visual pathway in the cortex [48-50]. There are also SNR local peaks in the calcarine sulcus in the EPI-EEG case, too, but the SNR is lower than that of SNS-InI-EEG and EEG-only case.
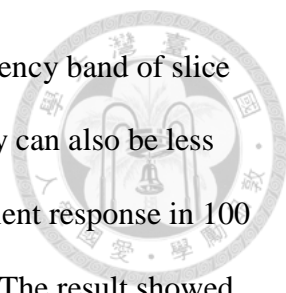
These results showed that interleaved SMS-InI-EEG reduces the effect of GA in specific frequency band. While the SNR distribution is similar in the SMS-InI-EEG and EEG-only case in V1 and V2, there are additional activations in the frontal lobe and temporal lobe near the auditory cortex in EPI-EEG case. These additional 15Hz signal in EPI-EEG case was not all related with the GA residue of EPI-EEG because the noise map was not overlapped with SNR map. In addition, no fMRI activity was shown in these additional areas. We thus concluded that the blip sound caused by gradient switching can induce unwanted EEG oscillations, but these activities were not high enough to evoke fMRI BOLD response.

31

Though superior in SNR than EPI-EEG, the SMS-InI-EEG still has an averagely lower SNR in V1 and V2 area than in EEG-only case (Fig. 3A). In addition, there was a wider range of high BOLD response vertices in SMS-InI. This was reported in previous work as a trait of InI that the dynamic changes in the direction of slice selection be spatially blurred [44]. This result also indicated a limitation of the effect of SMS in improving the spatial resolution of InI.

PA and GA are assumed independent because they exist in different frequency bands, and their appearance was not correlated in time [24, 25, 36]. Base on their independency, and that GA is excessively larger than PA, the residue of GA removal was preserved after PA removal. Thus the GA residue resulted in a lower in-band SNR in the SMS-InI-EEG case compared with the EEG-only case. Of the same reason, SMS-InI-EEG was less affected by GA and had less GA residue than EPI-EEG, so the SNR of SMS-InI-EEG was higher than EPI-EEG. Apart from that, because the source of GA and PA are independent, using interleaved SMS-InI-EEG won't change the amplitude and variation of PA. The reason why SMS-InI-EEG had better quality SSVEP was mainly that there was less GA residue in SMS-InI-EEG than in EPI-EEG. We discussed only the case using our artifact removal protocol. There might be different outcome when using other protocols, but the merit of interleaved SMS-InI-EEG remains when GA residue cannot be fully removed.

We used narrow band SSVEP to verify the improvement of EEG SNR using interleaved SMS-InI-EEG. There was N1 response on 200 ms, then the 15Hz quasi-sinusoidal SSVEP can be observed till 1200 ms. The SSVEP delayed about 200 ms, which make it last after the stimuli ended. The delay was observed in previous transient state SSVEP experiments [48, 62], can be ranged in 20 to 200 ms. Besides the narrow band SSVEP, broad band responses like the VEP response are also common responses

32

in EEG studies [29, 31, 32, 63]. Our method reduces GA in the frequency band of slice selection, so the broad band EEG responses containing this frequency can also be less affected by GA, and preserve more event related response. The transient response in 100 ms to 250 ms of our SSVEP was also a broad band response (Fig.3). The result showed that the peak of the transient response can be higher in the interleaved SMS-InI-EEG case than the EPI-EEG case.

The reliability of integrating EEG and fMRI data was based on the quality of both EEG and fMRI. Both of EEG and fMRI require a high SNR. Moreover, EEG targets a milliseconds resolution for identifying brain waves when fMRI targets a millimeter spatial resolution, full brain FOV, and a time resolution in seconds for locating brain activities.

Improvement in EEG or fMRI technique can either promote the quality of EEG-fMRI integration. However, improving the SNR of EEG is the most crucial when EEGs are concurrently recorded with fMRI because EEGs are contaminated by GA and PA in this case. Our method reduce GA and improve SNR of EEG with interleaved SMS-InI-EEG which cause less GA in EEG by using a new fMRI scanning sequence.

Previously, there were roughly three ways to reduce GA by changing EPI sequence, including spike driven EEG-fMRI[64-67], interleaved EPI-EEG [68-71], or using stepping stone sampling[72, 73].

The spike driven fMRI makes MRI scan starts after the offset of each EEG activities. When it takes 3 to 5 seconds to reach the peak of BOLD response, this fMRI can still get the BOLD responses of corresponding EEG activities. Unfortunately, it takes 3 to 4 scans to make T1 equilibrium saturate, which makes the first 3 to 4 scans have non-uniform contrasts[49, 72] and biases the estimation of BOLD responses. This problem was avoided when using continuous scan protocols like traditional EPI or using

33

our method, that the first few scans were excluded. For another thing, using spike driven fMRI cannot reduce GA during fMRI scans. This may result in EEG data loss when observing unpredictable spontaneous responses because the responses may appeared during acquisition[49, 72].

Interleaved EPI-EEG is done by reducing EPI slice number or making pauses after each full brain scans and reduced GA [68]. The reduced slices of EPI can be compressed[68-70] or equally distributed in each TR[71], and improve the duty cycle of EEG to 80 %[68-71]. However, reducing slice number results in a trade-off between FOV or slice thickness. On the other hand, making pauses after each scan increases the duty cycle of EEG equal to the ratio of TA and TR when preserving FOV and slice thickness. Yet it increase the TR of fMRI, and make the estimation of BOLD response less accurate. In comparison, interleaved SMS-InI-EEG maintained the FOV and sampling rate of fMRI in the cost of spatial resolution in the direction of slice selection.

The stepping stone sampling method makes the EEG samples between each gradient switching thus avoid the majority of GA on EEG [72]. This maintains the FOV, spatial resolution and sampling rate of fMRI while improving the EEG SNR. Yet the speed of gradient switching limited the sampling rate of EEG to less than 1000Hz in this setting [71]. Moreover, there is still errors between the samplings of EEG and the gaps of gradient switching, thus the GA cannot be totally avoided[67]. The degraded GAs are still in the frequency of slice selection, which affect the in-band SNR of EEG [74]. Instead, our method minimally sacrificed the spatial resolution of fMRI in the direction of slice selection, but maintained the in-band SNR of EEG.

In this work, same GA subtraction process was implemented on both EPI-EEG and SMS-InI-EEG. However, the SMS-InI-EEG was only contaminated by GA in 100 ms of each 2s TR, and about 80% of the EEG was almost not contaminated. So the EEG

signals in the contaminated time zones can possibly approximated by EEG signals in the artifact-free time zones[75]. This may further improve the SNR of EEG signal in concurrent EEG-fMRI.
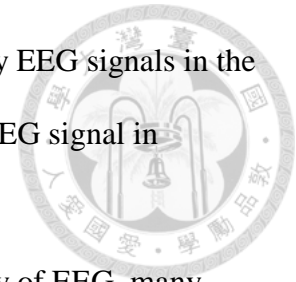
Different application of EEG-fMRI demands different quality of EEG, many EEG experiments uses spectral components of EEG as a marker of cognitive or mental states [76-79]. Our result showed that the SNR of EPI-EEG can be affected in near 15Hz, which locates in the range of beta wave (12~30Hz) and turns out biasing the estimation of beta activities[77, 80]. A slice of 3.5 to 4 mm is adequate for common cognitive neuroscientific experiments [81], and the height of human brain is about 120 mm. So the number of slices can be 30 to 35 in this condition, and the resulting GA is in the range of 15 to 17.5Hz. Thus using SMS-InI-EEG can ameliorate the bias on estimating beta activities. Moreover, the studies on single trial responses or spontaneous responses limit the power of averaging of EEG responses, so these studies require a lower noise level. Single trial responses, like the response evoked by a film, have usually longer length than artificial stimuli. So it may be impractical to replicate trials of each controlled conditions. In addition, the memory or study effect may be different between repetitions. So averaging the response of each trials may not be accepted [13, 20]. Spontaneous response, like the IID, has unpredictable onset and duration, and can be sparse in time[66, 82]. The SNR of it also cannot be increased by averaging each responses. Increasing the SNR of EEG acquisition is demanded in the mentioned situations, where interleaved SMS-InI-EEG can be helpful. On the other hand, the lower fMRI spatial resolution limits the application of SMS-InI-EEG on studying delicate spatial pattern of activities. For example, it require 2 mm fMRI resolution for discerning activities at different cortical layers[74].

Chapter 5. Appendices

5-A. Average artifact subtraction [25]

For each EEG channels, the data was first up-sample to 20 KHz and separated into segments by onsets of scans. The term "scan segments" refers to those segments of EEG. The first channel was used to align the scan segments. The average waveform of scan segments was taken as a reference. Waveform of each segment was then shifted to maximize the correlation with the reference. The same shifting amount was then applied to every channels.

Each of the scan segments was a $1 \times q$ (q = interpolated time points spanning each scan, 40,000 in this case) vector. The GA template for each scan segments Y_j^h was then estimated as:

$$\mathbf{A}_j = \frac{1}{K} \sum_{l \in \mathrm{I}(j)} Y_l^h \qquad \text{Eq.3}$$

Where l = 1, 2… N as the segments number, $\boldsymbol{A}_j$ is a $1 \times$ q vector of the GA template for segment j, and l was an index of the different scan segments, Y_l^h, to be averaged. *I(j)* was an index function determines which segments were included in the average, which was ranged in [j-7, …, j-1, j+1, …, j +7] in this work, so the amount of included segment K was 15. The GA template, $\boldsymbol{A}_j$, was then scaled by a constant α_j to minimize the least square error between the GA template and the corresponding scan segment:

$$\alpha_j = \frac{\boldsymbol{A}_j\left(Y_j^h\right)^T}{\boldsymbol{A}_j \boldsymbol{A}_j^T} \qquad \text{Eq.4}$$

Subtracting the scaled GA template $\alpha_j \boldsymbol{A}_j$ from Y_j^h for each segments, the cleaned EEG channel with first stage remainder was calculated, denoted as Y^r.

36

5-B. Heart beat detection

As a prerequisite to removing PAs, QRS complexes was detected from EKG channel. The

EKG channel was first band-pass filtered from 7 to 40 Hz, than a moving average filter

of samples in 28 ms intervals was applied to suppress electromyogram noise[36, 83],

denoted as x^f. The detection of QRS complexes was based on the positive value of k-

Teager energy[84, 85], e^t, of filtered EKG signal x^f:

$$e^t = max([x^f(n)]^2 - x^f(n-k)x^f(n+k), 0) \qquad \text{Eq.5}$$

The main period k in samples was tuned to sensitize pulse related frequency band:

$$k = \frac{f_s}{4f_d} \qquad \text{Eq.6}$$

Where f_s was the sampling rate (down-sampled to 500 Hz) and f_d was the 10th

harmonic frequency of expected heart rate (enough for describing QRS complexes

[36]), which was set as 10Hz in this work.

An adaptive threshold was applied to e^t for detecting every 'r' peaks of the QRS

complexes [83]. The MFR threshold is calculated as the sum of three thresholds: 1) M-

the steep-slope threshold, 2) F- the integrated threshold and 3 R- the beat expectation

threshold. The 'r' peak is detected in certain time points that its k-Teager energy surpass

the summation of the three thresholds. The M threshold decreased in an interval 200 to

1200 ms after last 'r' detection to 60% of the M threshold at the last 'r' time point,

which prevented overestimation of 'r' peaks. A queue with the 5 last maximum e^t

values in last 5 seconds was updated at any new 'r' peak detection. M was set as the

mean value of the queue after the detection.

The F threshold was the integral of e^t scaled by 1/150, which raised when high

frequency signal was nearby. The R threshold was zero after last 'r' peak and decreased

37

in an interval $\frac{2}{3} R_m$ *to* R_m after that. A queue with the 5 last 'r-r' intervals was updated at any new 'r' peak detection. R_m was the mean value of the queue.

5-C. Optimal basis set (OBS) subtraction for pulse artifact [36]

The PA in each EEG channel was assumed to have few typical shapes, referred as basis, in an interval of time near each 'r' peaks, which can be determined by temporal PCA[36] . Each EEG channel was separated into sections centered at each 'r' peaks shifted forward in time by 210 ms and with range as 1.5 times median 'r-r' interval (*mRR*), referred as a pulse section Y_r^P (with size $1 \times mRR$), where r was the number of that section, $r \in [1, R]$, R was the total number of 'r' peaks detected. PA in each pulse section was modeled by PCA among all the pulse sections Y^P after removal the 1st order trend of each sections. Few top PCs were enough for modeling of PA in each pulse section, and top 4 PCs B^P (with size $= 4 \times mRR$) were selected as the bases of PAs in this work. Then top 4 PCs were scaled by a weighting vector $\boldsymbol{\beta}_r^P$ which the sum of the weighted PCs $\boldsymbol{\beta}_r^P B^P$ was optimally fitted with each pulse section, Y_r^P:
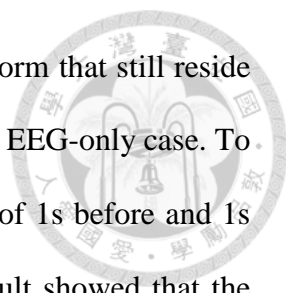
$$\boldsymbol{\beta}_r^P = (B^P (B^P)^T)^{-1} B^P (Y_r^P)^T \qquad\qquad \text{Eq.7}$$

Then the PAs $\boldsymbol{\beta}_r^P B^P$ were removed from each pulse section Y_r^P of a channel and the EEG channels, Y_r^C, with PAs cleaned was obtained:

$$Y_r^C = Y_r^P - \boldsymbol{\beta}_r^P B^P \qquad\qquad \text{Eq.8}$$

The OBS process was then applied to the next EEG channels until all the channels were clear from PAs.

The number of PCs used in modeling PAs was discussed in previous work[36]. More PCs can model more variations of the pulse sections. However, using more PCs in PA subtraction can also remove more stimulus response, especially when the responses

38

cannot be expected. We calculated the portion of average PA waveform that still reside in power after using different PCs in PA subtraction at Oz channel in EEG-only case. To exclude the stimulus responses, the pulse sections within the range of 1s before and 1s after the onset of stimuli were excluded in the calculation. The result showed that the portion of average PA waveform and its variation can be reduced more after using more PCs in PA subtraction, and using 4 PCs reduced the power to less than 1% (**Figure 6-A**). There were less than 0.1% power reduction using additional PC. Averaging among all channels, 86% of average PA waveforms were subtracted using 4 PCs in PA subtraction. This significant result was accordance with previous work [36].
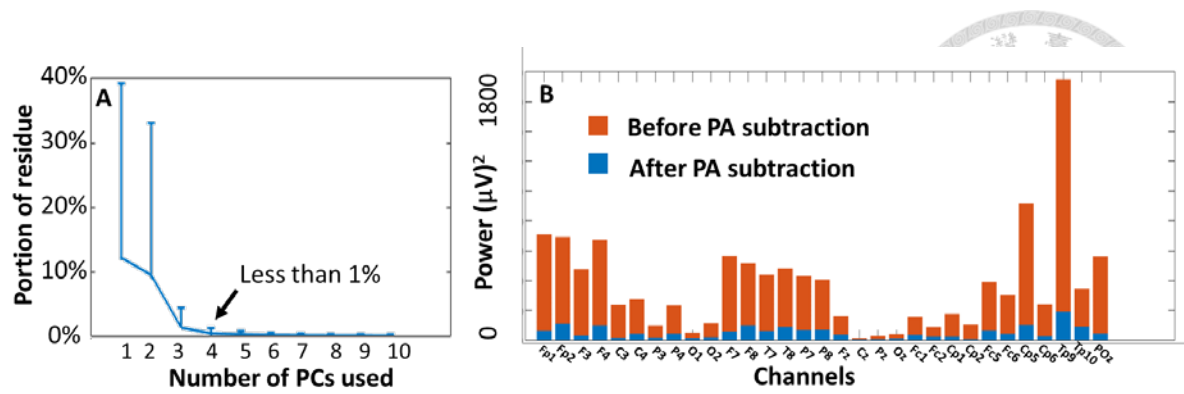
39

Figure 9 Portion of average power resided after PA removal. (A) PA residue in portion of power of average waveform of pulse sections in Oz channel. (B) Power of average PA waveform (orange bars) and power of average PA residue waveform (blue bars) in each channels. The pulse sections was averaged in sections before and after PA subtraction to form average waveform of PA and PA residue. The power of waveforms was calculated as mean square of waveforms in time.

40

References
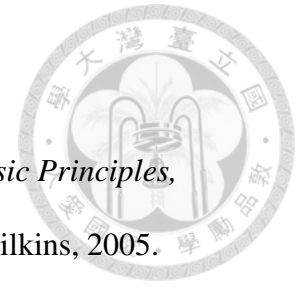
[1]   E. Niedermeyer, and F. H. L. da Silva, *Electroencephalography: Basic Principles, Clinical Applications, and Related Fields*: Lippincott Williams & Wilkins, 2005.

[2]   A. W. Toga, and J. C. Mazziotta, *Brain Mapping: The Methods*: Elsevier Science, 2002.

[3]   P. L. Nunez, *Electric Fields of the Brain: The Neurophysics of EEG*: Oxford University Press, 1981.

[4]   R. Ordidge, P. Mansfield, and R. Coupland, "Rapid biomedical imaging by NMR," *The British journal of radiology,* vol. 54, no. 646, pp. 850-855, 1981.

[5]   N. K. Logothetis, "What we can do and what we cannot do with fMRI," *Nature,* vol. 453, no. 7197, pp. 869-878, 2008.

[6]   R. J. Huster, S. Debener, T. Eichele, and C. S. Herrmann, "Methods for simultaneous EEG-fMRI: an introductory review," *The Journal of neuroscience,* vol. 32, no. 18, pp. 6053-6060, 2012.

[7]   C. Mulert, and L. Lemieux, *EEG - fMRI: Physiological Basis, Technique, and Applications*: Springer Berlin Heidelberg, 2009.

[8]   G. Lantz, R. G. De Peralta, L. Spinelli, M. Seeck, and C. Michel, "Epileptic source localization with high density EEG: how many electrodes are needed?," *Clinical neurophysiology,* vol. 114, no. 1, pp. 63-69, 2003.

[9]   M. A. Lindquist, J. M. Loh, L. Y. Atlas, and T. D. Wager, "Modeling the hemodynamic response function in fMRI: efficiency, bias and mis-modeling," *Neuroimage,* vol. 45, no. 1, pp. S187-S198, 2009.

[10]   R. B. Buxton, E. C. Wong, and L. R. Frank, "Dynamics of blood flow and oxygenation changes during brain activation: The balloon model," *Magnetic Resonance in Medicine,* vol. 39, no. 6, pp. 855-864, 1998.
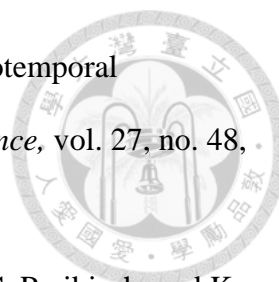
[11]   M. G. Philiastides, and P. Sajda, "EEG-informed fMRI reveals spatiotemporal characteristics of perceptual decision making," *Journal of Neuroscience,* vol. 27, no. 48, pp. 13082-13091, 2007.

[12]   H. Laufs, A. Kleinschmidt, A. Beyerle, E. Eger, A. Salek-Haddadi, C. Preibisch, and K. Krakow, "EEG-correlated fMRI of human alpha activity," *Neuroimage,* vol. 19, no. 4, pp. 1463-1476, 2003.

[13]   M. Ullsperger, and S. Debener, *Simultaneous EEG and fMRI: Recording, Analysis, and Application*: Oxford University Press, 2010.

[14]   F. Babiloni, F. Carducci, C. Del Gratta, C. Babiloni, G. Roberti, G. Romani, C. Caltagirone, P. Rossini, and A. Urbano, "Combined high resolution EEG and functional MRI data for modeling of cortical sources of human movement-related potentials." pp. 2135-2138.

[15]   F. Babiloni, F. Carducci, F. Cincotti, C. Del Gratta, G. Roberti, G. Romani, P. Rossini, and C. Babiloni, "Integration of high resolution EEG and functional magnetic resonance in the study of human movement-related potentials," *Methods Archive,* vol. 39, no. 2, pp. 179-182, 2000.

[16]   W. Ou, A. Nummenmaa, J. Ahveninen, J. W. Belliveau, M. S. Hämäläinen, and P. Golland, "Multimodal functional imaging using fMRI-informed regional EEG/MEG source estimation," *Neuroimage,* vol. 52, no. 1, pp. 97-108, 2010.

[17]   P. A. Valdes-Sosa, J. M. Sanchez-Bornot, R. C. Sotero, Y. Iturria-Medina, Y. Aleman-Gomez, J. Bosch-Bayard, F. Carbonell, and T. Ozaki, "Model driven EEG/fMRI fusion of brain oscillations," *Human brain mapping,* vol. 30, no. 9, pp. 2701-2721, 2009.

[18]   M. Rosa, J. Daunizeau, and K. Friston, "EEG-fMRI integration: a critical review of biophysical modeling and data analysis approaches," *Journal of integrative neuroscience,* vol. 9, no. 04, pp. 453-476, 2010.
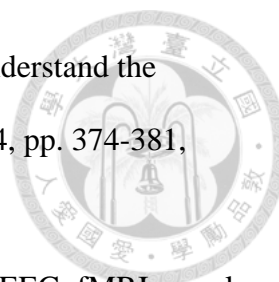
[19]　J. J. Riera, and A. Sumiyoshi, "Brain oscillations: ideal scenery to understand the neurovascular coupling," *Current opinion in neurology,* vol. 23, no. 4, pp. 374-381, 2010.

[20]　S. Debener, M. Ullsperger, M. Siegel, and A. K. Engel, "Single-trial EEG–fMRI reveals the dynamics of cognitive function," *Trends in cognitive sciences,* vol. 10, no. 12, pp. 558-563, 2006.

[21]　G. Sammer, C. Blecker, H. Gebhardt, P. Kirsch, R. Stark, and D. Vaitl, "Acquisition of typical EEG waveforms during fMRI: SSVEP, LRP, and frontal theta," *Neuroimage,* vol. 24, no. 4, pp. 1012-1024, 2005.

[22]　J. A. Caldwell, B. Prazinko, and J. L. Caldwell, "Body posture affects electroencephalographic activity and psychomotor vigilance task performance in sleep-deprived subjects," *Clinical Neurophysiology,* vol. 114, no. 1, pp. 23-31, 2003.

[23]　J. Jorge, F. Grouiller, Ö. Ipek, R. Stoermer, C. M. Michel, P. Figueiredo, W. Van Der Zwaag, and R. Gruetter, "Simultaneous EEG–fMRI at ultra-high field: Artifact prevention and safety assessment," *NeuroImage,* vol. 105, pp. 132-144, 2015.

[24]　P. J. Allen, G. Polizzi, K. Krakow, D. R. Fish, and L. Lemieux, "Identification of EEG events in the MR scanner: the problem of pulse artifact and a method for its subtraction," *Neuroimage,* vol. 8, no. 3, pp. 229-39, Oct, 1998.

[25]　P. J. Allen, O. Josephs, and R. Turner, "A method for removing imaging artifact from continuous EEG recorded during functional MRI," *Neuroimage,* vol. 12, no. 2, pp. 230-9, Aug, 2000.

[26]　X. Wan, K. Iwata, J. Riera, M. Kitamura, and R. Kawashima, "Artifact reduction for simultaneous EEG/fMRI recording: Adaptive FIR reduction of imaging artifacts," *Clinical Neurophysiology,* vol. 117, no. 3, pp. 681-692, 3//, 2006.

[27]   R. Ordidge, P. Mansfield, M. Doyle, and R. Coupland, "Real time movie images by NMR," *The British journal of radiology,* vol. 55, no. 658, pp. 729-733, 1982.

[28]   H. Berger, "Über das Elektrenkephalogramm des Menschen," *European Archives of Psychiatry and Clinical Neuroscience,* vol. 94, no. 1, pp. 16-60, 1931.

[29]   A. I. Klistorner, S. L. Graham, J. R. Grigg, and F. A. Billson, "Multifocal topographic visual evoked potential: improving objective detection of local visual field defects," *Investigative ophthalmology & visual science,* vol. 39, no. 6, pp. 937-950, 1998.

[30]   R. G. Eason, "Visual evoked potential correlates of early neural filtering during selective attention," *Bulletin of the Psychonomic Society,* vol. 18, no. 4, pp. 203-206, 1981.

[31]   F. Di Russo, A. Martínez, M. I. Sereno, S. Pitzalis, and S. A. Hillyard, "Cortical sources of the early components of the visual evoked potential," *Human brain mapping,* vol. 15, no. 2, pp. 95-111, 2002.

[32]   E. Courchesne, S. A. Hillyard, and R. Galambos, "Stimulus novelty, task relevance and the visual evoked potential in man," *Electroencephalography and Clinical Neurophysiology,* vol. 39, no. 2, pp. 131-143, 8//, 1975.

[33]   V. P. Clark, S. Fan, and S. A. Hillyard, "Identification of early visual evoked potential generators by retinotopic and topographic analyses," *Human brain mapping,* vol. 2, no. 3, pp. 170-187, 1994.

[34]   A. Hoffmann, L. Jäger, K. Werhahn, M. Jaschke, S. Noachtar, and M. Reiser, "Electroencephalography during functional echo-planar imaging: detection of epileptic spikes using post-processing methods," *Magnetic resonance in medicine,* vol. 44, no. 5, pp. 791-798, 2000.

[35]   G. Bonmassar, P. L. Purdon, I. P. Jääskeläinen, K. Chiappa, V. Solo, E. N. Brown, and J. W. Belliveau, "Motion and ballistocardiogram artifact removal for interleaved

recording of EEG and EPs during MRI," *Neuroimage,* vol. 16, no. 4, pp. 1127-1141, 2002.

[36]   R. K. Niazy, C. F. Beckmann, G. D. Iannetti, J. M. Brady, and S. M. Smith, "Removal of FMRI environment artifacts from EEG data using optimal basis sets," *NeuroImage,* vol. 28, no. 3, pp. 720-737, 11/15/, 2005.

[37]   D. Maziero, T. R. Velasco, N. Hunt, E. Payne, L. Lemieux, C. E. Salmon, and D. W. Carmichael, "Towards motion insensitive EEG-fMRI: Correcting motion-induced voltages and gradient artefact instability in EEG using an fMRI prospective motion correction (PMC) system," *NeuroImage,* vol. 138, pp. 13-27, 2016.

[38]   G. Bonmassar, D. P. Schwartz, A. K. Liu, K. K. Kwong, A. M. Dale, and J. W. Belliveau, "Spatiotemporal brain imaging of visual-evoked activity using interleaved EEG and fMRI recordings," *Neuroimage,* vol. 13, no. 6 Pt 1, pp. 1035-43, Jun, 2001.

[39]   R. I. Goldman, J. M. Stern, J. Engel Jr, and M. S. Cohen, "Simultaneous EEG and fMRI of the alpha rhythm," *Neuroreport,* vol. 13, no. 18, pp. 2487, 2002.

[40]   W. X. Yan, K. J. Mullinger, M. J. Brookes, and R. Bowtell, "Understanding gradient artefacts in simultaneous EEG/fMRI," *Neuroimage,* vol. 46, no. 2, pp. 459-471, 2009.

[41]   H. Mandelkow, P. Halder, P. Boesiger, and D. Brandeis, "Synchronization facilitates removal of MRI artefacts from concurrent EEG recordings and increases usable bandwidth," *Neuroimage,* vol. 32, no. 3, pp. 1120-1126, 2006.

[42]   P. Ritter, F. Freyer, G. Curio, and A. Villringer, "High-frequency (600 Hz) population spikes in human EEG delineate thalamic and cortical fMRI activation sites," *Neuroimage,* vol. 42, no. 2, pp. 483-490, 2008.

[43]   M. Barth, F. Breuer, P. J. Koopmans, D. G. Norris, and B. A. Poser, "Simultaneous multislice (SMS) imaging techniques," *Magnetic resonance in medicine,* vol. 75, no. 1, pp. 63-81, 2016.
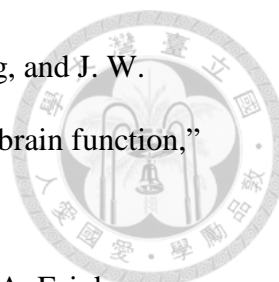
[44] F. H. Lin, L. L. Wald, S. P. Ahlfors, M. S. Hämäläinen, K. K. Kwong, and J. W. Belliveau, "Dynamic magnetic resonance inverse imaging of human brain function," *Magnetic resonance in medicine,* vol. 56, no. 4, pp. 787-802, 2006.

[45] L. Chen, A. T. Vu, J. Xu, S. Moeller, K. Ugurbil, E. Yacoub, and D. A. Feinberg, "Evaluation of highly accelerated simultaneous multi-slice EPI for fMRI," *NeuroImage,* vol. 104, pp. 452-459, 2015/01/01/, 2015.

[46] K. P. Pruessmann, M. Weiger, M. B. Scheidegger, and P. Boesiger, "SENSE: Sensitivity encoding for fast MRI," *Magnetic Resonance in Medicine,* vol. 42, no. 5, pp. 952-962, 1999.

[47] D. A. Feinberg, and K. Setsompop, "Ultra-fast MRI of the human brain with simultaneous multi-slice imaging," *Journal of Magnetic Resonance,* vol. 229, pp. 90-100, 2013/04/01/, 2013.

[48] A. M. Norcia, L. G. Appelbaum, J. M. Ales, B. R. Cottereau, and B. Rossion, "The steady-state visual evoked potential in vision research: a review," *Journal of vision,* vol. 15, no. 6, pp. 4-4, 2015.

[49] C. S. Herrmann, "Human EEG responses to 1–100 Hz flicker: resonance phenomena in visual cortex and their potential correlation to cognitive phenomena," *Experimental brain research,* vol. 137, no. 3-4, pp. 346-353, 2001.

[50] A. Bayram, Z. Bayraktaroglu, E. Karahan, B. Erdogan, B. Bilgic, M. Özker, I. Kasikci, A. D. Duru, A. Ademoglu, C. Öztürk, K. Arikan, N. Tarhan, and T. Demiralp, "Simultaneous EEG/fMRI Analysis of the Resonance Phenomena in Steady-State Visual Evoked Responses," *Clinical EEG and Neuroscience,* vol. 42, no. 2, pp. 98-106, April 1, 2011, 2011.
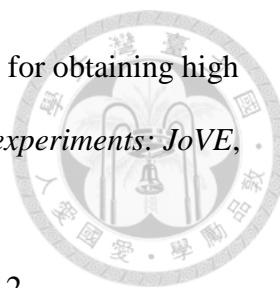
[51] K. J. Mullinger, P. Castellone, and R. Bowtell, "Best current practice for obtaining high quality EEG data during simultaneous fMRI," *Journal of visualized experiments: JoVE,* no. 76, 2013.

[52] B. Fischl, "FreeSurfer," *Neuroimage,* vol. 62, no. 2, pp. 774-781, 2012.

[53] A. Gramfort, M. Luessi, E. Larson, D. A. Engemann, D. Strohmeier, C. Brodbeck, L. Parkkonen, and M. S. Hämäläinen, "MNE software for processing MEG and EEG data," *NeuroImage,* vol. 86, pp. 446-460, 2014/02/01/, 2014.

[54] M. Stenroos, V. Mäntynen, and J. Nenonen, "A Matlab library for solving quasi-static volume conduction problems using the boundary element method," *Computer methods and programs in biomedicine,* vol. 88, no. 3, pp. 256-263, 2007.

[55] M. Stenroos, and A. Nummenmaa, "Incorporating and Compensating Cerebrospinal Fluid in Surface-Based Forward Models of Magneto- and Electroencephalography," *PLOS ONE,* vol. 11, no. 7, pp. e0159595, 2016.

[56] K. J. Friston, "Functional and Effective Connectivity: A Review," *Brain Connectivity,* vol. 1, no. 1, pp. 13-36, 2011/01/01, 2011.

[57] N. Roehri, J.-M. Lina, J. C. Mosher, F. Bartolomei, and C.-G. Bénar, "Time-frequency strategies for increasing high-frequency oscillation detectability in intracerebral EEG," *IEEE Transactions on Biomedical Engineering,* vol. 63, no. 12, pp. 2595-2606, 2016.

[58] S. Burnos, P. Hilfiker, O. Sürücü, F. Scholkmann, N. Krayenbühl, T. Grunwald, and J. Sarnthein, "Human intracranial high frequency oscillations (HFOs) detected by automatic time-frequency analysis," *PLoS One,* vol. 9, no. 4, pp. e94381, 2014.

[59] P. Goupillaud, A. Grossmann, and J. Morlet, "Cycle-octave and related transforms in seismic signal analysis," *Geoexploration,* vol. 23, no. 1, pp. 85-102, 1984/10/01/, 1984.

[60] C. F. Beckmann, M. Jenkinson, and S. M. Smith, "General multilevel linear modeling for group analysis in FMRI," *Neuroimage,* vol. 20, no. 2, pp. 1052-1063, 2003.

47
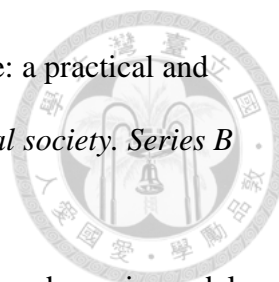
[61]　Y. Benjamini, and Y. Hochberg, "Controlling the false discovery rate: a practical and powerful approach to multiple testing," *Journal of the royal statistical society. Series B (Methodological)*, pp. 289-300, 1995.

[62]　S. Zhang, X. Han, X. Chen, Y. Wang, S. Gao, and X. Gao, "A study on dynamic model of steady-state visual evoked potentials," *Journal of neural engineering,* vol. 15, no. 4, pp. 046010, 2018.

[63]　B. A. Wandell, S. O. Dumoulin, and A. A. Brewer, "Visual field maps in human cortex," *Neuron,* vol. 56, no. 2, pp. 366-383, 2007.

[64]　S. Warach, J. Ives, G. Schlaug, M. Patel, D. Darby, V. Thangaraj, R. Edelman, and D. Schomer, "EEG-triggered echo-planar functional MRI in epilepsy," *Neurology,* vol. 47, no. 1, pp. 89-93, 1996.

[65]　K. Krakow, F. Woermann, M. Symms, P. Allen, L. Lemieux, G. Barker, J. Duncan, and D. Fish, "EEG-triggered functional MRI of interictal epileptiform activity in patients with partial seizures," *Brain,* vol. 122, no. 9, pp. 1679-1688, 1999.

[66]　F. Lazeyras, O. Blanke, S. Perrig, I. Zimine, X. Golay, J. Delavelle, C. M. Michel, N. De Tribolet, J. G. Villemure, and M. Seeck, "EEG-triggered functional MRI in patients with pharmacoresistant epilepsy," *Journal of Magnetic Resonance Imaging,* vol. 12, no. 1, pp. 177-185, 2000.

[67]　L. Lemieux, K. Krakow, and D. R. Fish, "Comparison of spike-triggered functional MRI BOLD activation and EEG dipole model localization," *Neuroimage,* vol. 14, no. 5, pp. 1097-1104, 2001.

[68]　G. Bonmassar, K. Anami, J. Ives, and J. W. Belliveau, "Visual evoked potential (VEP) measured by simultaneous 64-channel EEG and 3T fMRI," *NeuroReport,* vol. 10, no. 9, pp. 1893-1897, 1999.

[69] F. Kruggel, C. J. Wiggins, C. S. Herrmann, and D. Y. von Cramon, "Recording of the event-related potentials during functional MRI at 3.0 Tesla field strength," *Magnetic Resonance in Medicine: An Official Journal of the International Society for Magnetic Resonance in Medicine,* vol. 44, no. 2, pp. 277-282, 2000.

[70] F. Kruggel, C. S. Herrmann, C. J. Wiggins, and D. Y. von Cramon, "Hemodynamic and electroencephalographic responses to illusory figures: recording of the evoked potentials during functional MRI," *Neuroimage,* vol. 14, no. 6, pp. 1327-1336, 2001.

[71] R. I. Goldman, J. M. Stern, J. Engel Jr, and M. S. Cohen, "Acquiring simultaneous EEG and functional MRI," *Clinical Neurophysiology,* vol. 111, no. 11, pp. 1974-1980, 2000.

[72] K. Anami, T. Mori, F. Tanaka, Y. Kawagoe, J. Okamoto, M. Yarita, T. Ohnishi, M. Yumoto, H. Matsuda, and O. Saitoh, "Stepping stone sampling for retrieving artifact-free electroencephalogram during functional magnetic resonance imaging," *Neuroimage,* vol. 19, no. 2, pp. 281-295, 2003.

[73] F. Freyer, R. Becker, K. Anami, G. Curio, A. Villringer, and P. Ritter, "Ultrahigh-frequency EEG during fMRI: pushing the limits of imaging-artifact correction," *Neuroimage,* vol. 48, no. 1, pp. 94-108, 2009.

[74] N. K. Logothetis, "What we can do and what we cannot do with fMRI," *Nature,* vol. 453, pp. 869, 06/12/online, 2008.

[75] D. Needell, and J. A. Tropp, "CoSaMP: Iterative signal recovery from incomplete and inaccurate samples," *Applied and Computational Harmonic Analysis,* vol. 26, no. 3, pp. 301-321, 2009/05/01/, 2009.

[76] C. Michel, D. Lehmann, B. Henggeler, and D. Brandeis, "Localization of the sources of EEG delta, theta, alpha and beta frequency bands using the FFT dipole approximation," *Electroencephalography and clinical neurophysiology,* vol. 82, no. 1, pp. 38-44, 1992.
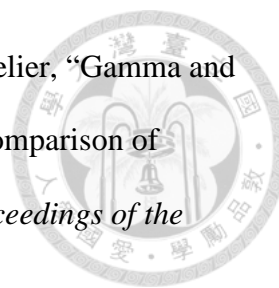
[77] C. Haenschel, T. Baldeweg, R. J. Croft, M. Whittington, and J. Gruzelier, "Gamma and beta frequency oscillations in response to novel auditory stimuli: a comparison of human electroencephalogram (EEG) data with in vitro models," *Proceedings of the National Academy of Sciences,* vol. 97, no. 13, pp. 7645-7650, 2000.

[78] A. K. Roopun, S. J. Middleton, M. O. Cunningham, F. E. N. LeBeau, A. Bibbig, M. A. Whittington, and R. D. Traub, "A beta2-frequency (20–30 Hz) oscillation in nonsynaptic networks of somatosensory cortex," *Proceedings of the National Academy of Sciences,* vol. 103, no. 42, pp. 15646-15650, 2006.

[79] S. R. Jones, C. E. Kerr, Q. Wan, D. L. Pritchett, M. Hämäläinen, and C. I. Moore, "Cued Spatial Attention Drives Functionally-Relevant Modulation of The Mu Rhythm in Primary Somatosensory Cortex," *The Journal of neuroscience : the official journal of the Society for Neuroscience,* vol. 30, no. 41, pp. 13760-13765, 2010.

[80] N. Swann, H. Poizner, M. Houser, S. Gould, I. Greenhouse, W. Cai, J. Strunk, J. George, and A. R. Aron, "Deep brain stimulation of the subthalamic nucleus alters the cortical profile of response inhibition in the beta frequency band: a scalp EEG study in Parkinson's disease," *Journal of Neuroscience,* vol. 31, no. 15, pp. 5721-5729, 2011.

[81] G. H. Glover, "Overview of functional magnetic resonance imaging," *Neurosurgery Clinics,* vol. 22, no. 2, pp. 133-139, 2011.

[82] J. Gotman, and F. Pittau, "Combining EEG and fMRI in the study of epileptic discharges," *Epilepsia,* vol. 52, no. s4, pp. 38-42, 2011.

[83] I. I. Christov, "Real time electrocardiogram QRS detection using combined adaptive threshold," *Biomedical engineering online,* vol. 3, no. 1, pp. 28, 2004.

[84] K. H. Kim, H. W. Yoon, and H. W. Park, "Improved ballistocardiac artifact removal from the electroencephalogram recorded in fMRI," *Journal of neuroscience methods,* vol. 135, no. 1, pp. 193-203, 2004.

[85]   P. Maragos, J. F. Kaiser, and T. F. Quatieri, "On amplitude and frequency demodulation using energy operators," *IEEE Transactions on signal processing,* vol. 41, no. 4, pp. 1532-1550, 1993.